JOURNAL OF MATERIALS SCIENCE 33 (1998) 1319–1324

Tensile ductility behaviour of fine-grained alumina at elevated temperature

WOO JIN KIM
Department of Metallurgy Engineering and Materials Science, Hong-Ik University, 72-1, Sangsu-dong, Mapo-Ku, Seoul, 121-791, Korea

O. D. SHERBY
Department of Materials Science and Engineering, Stanford University, Stanford, CA 94305, USA

High-temperature tensile ductility behaviour of polycrystalline fine-grained alumina is shown to be classified into four regimes, depending on flow stress: (1) fast-crack growth regime, (2) single-crack growth regime, (3) microcracks growth regime, and (4) superplastic-crack growth regime, in the order of decreasing flow stress. The unique tensile ductility behaviour observed for each fracture regime is related to the type of damage accumulation. A fracture mechanics model is applied to interpret the tensile ductility of alumina in the superplastic-crack growth regime. The model correctly predicts the observed linear decrease in the true fracture strain with an increase in the logarithm of flow stress. In addition, the model is in quantitative agreement with the increase in the true fracture strain with decreasing grain size when compared at a given stress. The enhancement of tensile ductility in alumina by dilute MgO additions is attributed to an increase in the surface energy and/or decrease in the grain-boundary energy which resists the fracture process. On the other hand, the enhancement of tensile ductility in alumina by addition of a second phase of zirconia is attributed to an increase in the amount of alumina–zirconia grain boundaries which have a low grain-boundary energy.

1. Introduction

Studies on the creep behaviour of alumina are extensive [1–4]. Diffusional creep, grain-boundary sliding and dislocation glide and climb have been considered as mechanisms that control plastic flow in alumina at elevated temperature [3–5]. Studies on the tensile ductility behaviour of alumina, on the other hand, have been limited. It is only in recent years that this property has been explored in some detail. These studies have centred on fracture strain evaluation by flexure or by uniaxial tension tests.

Dalgleish *et al.* [6] in 1985, performed a number of flexure tests on an alumina material containing 0.25 wt % MgO in solid solution, with a grain size of 4 μm, in the temperature range, 1250–1300 °C. They showed that the flexural ductility is a function of stress, increasing with a decrease in stress. They identified two regimes of fracture behaviour: a slow-crack growth regime at high stresses and a creep-damage regime at low stresses. A maximum flexural ductility of 18% was observed. Gruffel *et al.* [7] in 1988, performed tension tests 1450 °C on several alumina materials containing small amounts of MgO plus other additives such as Y_2O_3 and Cr_2O_3. They observed tensile ductility values as high as 65%. In 1989, Wakai and co-workers [8, 9] showed very high tensile elongations (as high as 120%) when alumina contains a second phase of yttria-stabilized zirconia. The authors considered that grain-boundary sliding was a principal mechanism of deformation. Wilkinson *et al.* [10, 11], in 1991, conducted flexure and tension tests on alumina materials containing small amounts of MgO and Y_2O_3 in solid solution, with grain sizes in the range of 1–1.6 μm, at temperatures ranging from 1150–1250 °C. The authors concluded that flexure studies did not yield true tensile fracture strain behaviour because of the stress gradient in flexure tests. In addition, Wilkinson *et al.* identified three different fracture regimes based on observations of damage characteristics: (1) a slow-crack growth regime at high stresses (2) a microcracks growth regime at intermediate stresses and (3) a damage-tolerance regime at low stresses. Tensile elongations ranging from 1%–27% were observed. Yoshizawa and Sakuma [12, 13], in 1992 and 1994, carried out tension tests on an alumina material containing 0.1 wt % MgO with a grain size of 0.8 μm. Their tests were conducted at high temperatures, between 1300 and 1550 °C, and large tensile elongations in the order of 80% were observed. The authors showed that dilutely alloyed alumina, containing MgO, was more ductile than pure alumina. This difference was explained by an inhibition of grain

growth during deformation from the presence of MgO.

It is the purpose of this paper to compare all the high-temperature fracture strain data for fine-grained alumina materials and to establish a unified view of their tensile ductility behaviour as a function of flow stress. The objective of such a study is to understand better the tensile ductility behaviour of alumina as well as other fine-grained ceramics.

2. Tensile ductility of polycrystalline ceramics compared with alumina

It has been shown that the tensile ductility of superplastic ceramics is a strong function of the flow stress at elevated temperature, increasing with a decrease in the flow stress [14, 15]. Specifically, a linear correlation was found between the true fracture strain, ε_f, and the logarithm of flow stress, σ, for a number of superplastic ceramics in the temperature and stress range where the strain-rate sensitivity exponent, m, is high ($m \geqslant 0.5$ in the flow stress, σ, and strain rate, $\dot{\varepsilon}$, relation $\sigma = k\dot{\varepsilon}^m$).

Fig. 1 shows the linear correlation between true fracture strain and logarithm of flow stress for various superplastic ceramics reported to date, excluding alumina. The data were obtained from the literature [15–30]. It can be noted from the plot that all the different ceramic materials exhibit a similar value of the slope. This slope is related to the rate of damage accumulation as a function of plastic strain from the common deformation mechanism of grain-boundary sliding [14, 15]. The difference in tensile ductility at a given flow stress for the various ceramic materials has been attributed to differences in grain size, elastic modulus, as well as to the difference in the surface and grain-boundary energies [14, 15].

Fig. 2 is a similar correlation to that shown in Fig. 1 for various alumina materials. In the plot, four regimes are identified depending on flow stress. These regimes can be summarized as follows.

At very high stresses, Regime I, no plastic straining is predicted and classical fracture mechanics theory is applicable. In Regime II, very low plastic strains are observed, typically less than 1%, and this regime is related to failure driven by growth of a single crack. In Regime III, the fracture strain is seen to be insensitive to the flow stress with tensile elongations in the order of 10%. Finally, in Regime IV, the low-stress range, the fracture strain is seen to be a strong function of flow stress, with a slope essentially equal to the slopes observed in fine-grained superplastic ceramics as shown in Fig. 1.

The data shown in Fig. 2 are for alumina containing various dilute solid solution additions as well as, in three cases, alumina containing various amounts of a second phase (yttria-stabilized zirconia). Table I lists the composition of the alumina materials evaluated, and includes the grain size, temperature, methods of testing, true fracture strain and the symbols used to describe the data in Fig. 2. The alumina materials, listed in Table I, are divided into four groups. The first group (A) consists of alumina materials with a small amount of MgO (200–500 p.p.m.). The second group (B) consists of alumina materials with a substantial amount of MgO (0.1–0.3 wt %). The third group (C) consists of alumina as well as alumina containing 7.3 wt % yttria-stabilized zirconia (3Y-TZP); the alumina, in both cases, is in a highly pure state. The fourth group consists of two alumina composites with 18–22 wt % yttria stabilized zirconia (3Y-TZP).

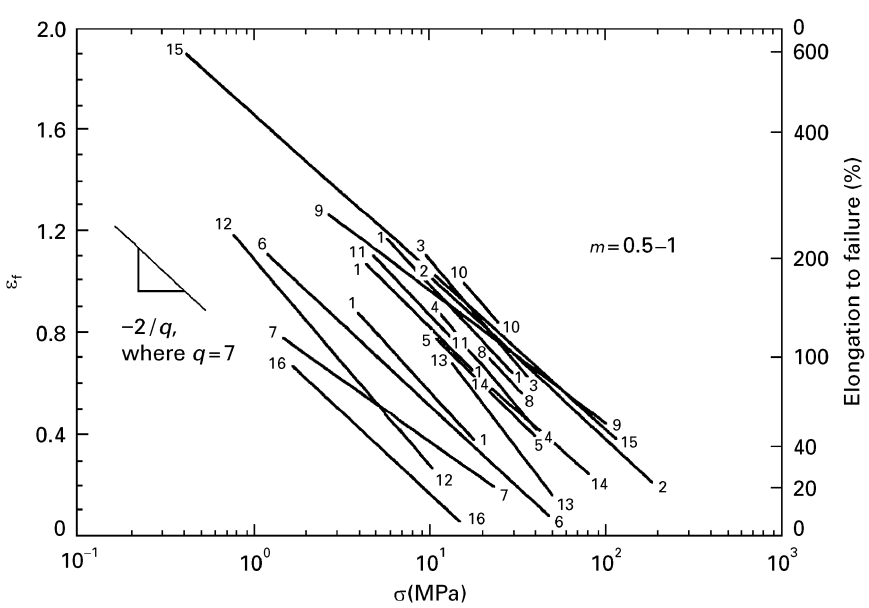

Figure 1 Influence of low stress on the true fracture strain for fine-grained polycrystalline ceramics in the temperature range where the strain-rate sensitivity exponent, m, is high ($m \geqslant 0.5$). 1, Y-TZP (1350–1550 °C)[16–20]. 2, Y-TZP + 20 wt% Al_2O_3 (1350–1500 °C)[21]. 3, Y-TZP + 40 wt% Al_2O_3 (1450–1550 °C)[9]. 4, Y-TZP + 60 wt% Al_2O_3 (1450–1550 °C)[9]. 5, Y-TZP + 80 wt% Al_2O_3 (1450–1550 °C)[9]. 6, $PbTiO_3$ (950–1150 °C)[22]. 7, β–spodumene glass (1100–1150 °C)[23]. 8, Si_3N_4/SiC (1600 °C)[24]. 9, 3Mn–2.6Y–TZP [25]. 10, Hydroxyapatite (1000–1100 °C)[26]. 11, 2Y-TZP (1450 °C)[27]. 12, β–SiAlON (1550 °C)[28]. 13, Al_2O_3–Y_2O_3–Si_3N_4/SiC (1575–1650 °C)[29]. 14, 0.1 wt% MgO–Al_2O_3 (1300–1450 °C)[12, 13]. 15, Fe_3C + 20 Fe (725–1050 °C)[30]. 16, $Fe_3AlC_{0.5}$ + 10 FeAl (950–1250 °C)[31].

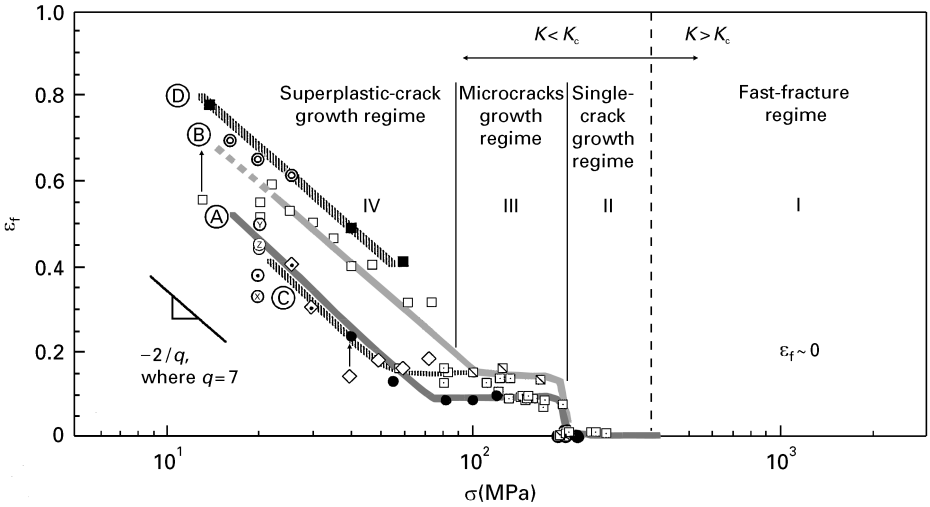

Figure 2 Influence of flow stress on the true fracture strain for fine-grained alumina. For key, see Table I.

The following section discusses the tensile ductility behaviour of these alumina materials in detail. All the fine-grained alumina materials were observed to exhibit a high strain-rate sensitivity exponent, ~ 0.5, in the temperature and stress ranges where the flexure or tension tests were conducted.

3. Discussion

3.1. Influence of stress on tensile ductility of fine-grained alumina

It is generally accepted that fine-grained alumina materials fracture in a brittle manner without neck formation. It is, therefore, important to consider cavitation and crack nucleation and propagation in order to understand the fracture strain results for fine-grained alumina materials. This cavitation and crack behaviour is believed to be related to the flow stress and will be discussed in the following sections.

3.1.1. Fast-fracture regime (Regime I)

When an applied stress is such that a stress intensity factor, K, is equal to or larger than the critical stress intensity factor, K_c, fracture occurs instantaneously upon loading [32]. This is the case for fast fracture. The fracture stress, σ_f, for the beginning of fast fracture can be determined from the relation; $\sigma_f = K_c/(\pi c^*)^{1/2}$ where c^* is the largest crack size. The critical stress for fast fracture can be calculated if K_c at elevated temperatures is known and the critical pre-existing crack size is known. This allows prediction of the boundary between Regime I and Regime II shown in Fig. 2. No experimental studies have been made to confirm the predicted bound. The critical stress intensity factor for alumina, K_c, can be obtained by using the Gilman relation for K_c, which is for fracture driven by an intergranular crack [33]. The Gilman relation for K_c is given by the following equation

$$K_c = [(2\gamma_s - \gamma_{gb})E]^{1/2} \quad (1)$$

where E is Young's modulus, and γ_s and γ_{gb} are surface and grain-boundary energies, respectively. The values of γ_s and γ_{gb} for commercially pure alumina were measured as a function of temperature by Nikolopoulos [34] using a multiphase equilibrium method. The values of γ_s and γ_{gb} are 1.37 and 0.93 $J\,m^{-2}$, respectively, at a temperature of 1250 °C. Young's modulus for alumina at 1250 °C is 2.3×10^5 MPa [35]. Thus, the value of K_c calculated by this method is 0.65 $MN\,m^{-3/2}$. The value of C^* was selected as 1 μm, based on the typical grain size studied by all investigators (Table I) on the commonly used assumption that the critical crack size is equal to the grain size. This calculation leads to $\sigma_f = 364$ MPa and was to set the boundary between Regime I and II shown in Fig. 2.

3.1.2. Single-crack growth regime (Regime II)

In Regime II, the largest pre-existing crack grows rapidly to the critical size before general plastic deformation occurs. Crack growth is controlled by nucleation and growth of cavities in the zone ahead of the crack tip where high elastic stresses are concentrated. The cavities are only observed ahead of the largest crack. Models for this process [36–38] have been well established and predict that crack growth is related to a deformation time, t, a stress intensity factor, K, and a diffusion rate, D. Typically, only small fracture strains, less than 1% elongation, are observed in Regime II.

3.1.3. Microcracks growth regime (Regime III)

At intermediate stresses, a number of microcracks and cavities are observed. Microcracks remain sharp as they grow and most cavities are flat or crack-like [10, 11]. Failure in this regime involves the growth and linkage of microcracks and cavities. The creation of new cavities and cracks is a result of stress relaxation at pre-existing cracks. This is because the material deforms slowly under the lower stresses in Regime III compared to the stresses in Regime II. This stress

TABLE I Tensile and flexural ductility of various alumina materials investigated at elevated temperatures

Materials (T, tension; F, flexure) Al_2O_3 + additives or second phase	Reference	Grain size (μm)	Temperature (°C)	True fracture strain (ε_f)
A: Alumina containing a small amount of MgO				
Symbol: ○⊙⊗ (T) 500 p.p.m. MgO	Gruffel *et al.* [7]	0.77–1.5	1450	0.3–0.45
Symbol: ▲ (T) 500 p.p.m. MgO + 500 p.p.m. Y_2O_3	Gruffel *et al.* [7]	0.66	1450	0.5
Symbol: ◇ (T) 500 p.p.m. MgO + 1 wt % Cr_2O_3	Gruffel *et al.* [7]	0.83	1450	0.44
Symbol: ● (T) ● (F) 200 p.p.m. MgO + 800 p.p.m. Y_2O_3	Robertson *et al.* [11]	1	1250	< 0.25
B: Alumina containing a large amoung of MgO				
Symbol: □ (F) 0.25 wt % MgO	Dalgleish *et al.* [6]	4	1250–1300	< 0.2
Symbol: ⧅ (F) 0.3 wt % MgO	Robertson *et al.* [11]	1.6	1150	< 0.2
Symbol: □ (T) 0.1 wt % MgO	Yoshizawa *et al.* [12, 13]	0.8	1300–1450	0.3–0.55
C: Pure alumina and alumina composite				
Symbol: ⊘ (T) Pure	Yoshizawa *et al.* [12, 13]	0.9	1300–1450	0.15–0.2
Symbol: ⊖ (T) 7.3 wt % Y-ZrO_2	Kuroishi *et al.* [8]	0.77–0.94	1450	0.3–0.4
D: Alumina/yttria-stabilized zirconia (Y-ZrO_2) composite				
Symbol: ■ (T) 20 wt % Y-ZrO_2	Wakai *et al.* [8]	1	1450–1550	0.4–0.8
Symbol: ● (T) 18–22 wt % Y-ZrO_2	Kuroishi *et al.* [8]	0.66–0.86	1450	0.6–0.7

relaxation decreases the rate of growth of the largest pre-existing cracks and allows for the nucleation and growth of other new microcracks and cavities. General plastic flow can occur probably involving both slip and grain-boundary sliding. Tensile elongations in Regime III are typically 6%–13%, and appear to be insensitive to the flow stress (Fig. 2). No mechanistic explanations have been proposed for this trend between ε_f and σ. It is similar to the Monkman–Grant phenomenological relation for creep of metallic materials where ε_f is shown to be constant independent of stress [39]. It is proposed that the tensile ductility in Regime III is controlled by contributions from two competing mechanisms. These are: single-crack growth of the type described in Regime II and of superplastic-crack growth of the type to be described in Regime IV.

3.1.4. Superplastic-crack growth regime (Regime IV)

The large elongations observed in Regime IV are a result of the high degree of blunting of cavities and cracks occurring in a highly relaxed material [7, 10, 11, 15]. This blunting of cracks and cavities will significantly retard crack and cavity interlinkage processes. Cavities are fully relaxed, and spherical-shaped cavities are frequently observed. Thus, a high extent of damage can be tolerated before final fracture occurs. Damage will occur through grain-boundary sliding which is believed to be the principal deformation mechanism in fine-grained superplastic ceramic materials. Plastic straining during grain-boundary sliding will lead to cavity nucleation and growth. This is because cavities will nucleate at stress concentration areas such as triple points of grains or grain-boundary ledges where grain-boundary sliding is impeded.

Kim *et al.* developed a fracture mechanics model based on the above concept [14]. They assumed that crack growth is driven by plastic strain, ε, according to $C = C_0 \exp(q\varepsilon)$. In this relation, C is the crack size, C_0 is the initial crack size which is related to the grain size, and q is a material constant that determines the crack-growth rate during plastic strain. The fracture strain equation developed based on this crack-growth equation, together with a brittle fracture criterion (the critical stress intensity factor, K_c), led to the following fracture strain relation

$$\varepsilon_f = \ln\left(\frac{K_c}{\pi d}\sigma^{-2}\right)^{1/q} \quad (2)$$

where d is the grain size. Equation 2 predicts a unique relation between the true fracture strain, ε_f, and the flow stress for a given grain size. Analyses of all data for fine-grained superplastic ceramics yield an

approximately constant value of q equal to 7* as can be seen in Figs 1 and 2. The same approximate value of q for all superplastic ceramics indicates that q is probably related to fracture driven by the specific deformation mechanism of grain-boundary sliding.

The following observation can be noted regarding the tensile ductility data obtained in Regime IV. The fracture strain values observed by Yoshizawa and Sakuma [12] for pure alumina are considerably less than those observed by Kuroishi *et al.* [8] for pure alumina containing 7.3 wt % yttria-stabilized zirconia (3Y-TZP), even when compared at a comparable stress (Fig. 2). Both materials have about the same initial grain size. The reason for this difference is that large grain growth occurs in pure alumina during plastic deformation [12], leading to lower fracture strains than expected as a result of the coarser grain size. In the case of pure alumina with the second phase of Y-TZP, however, little grain growth is expected during plastic deformation, and hence high tensile ductility should be obtained. These results are in agreement with the predictions as given by Equation 2. The unexpected low fracture strain observed at low stresses for an alumina containing 0.1 wt % MgO may also be attributed to the large grain growth that occurred during deformation [12].

As a final point, it should be noted that the highest fracture-strain datum point of Robertson *et al.* [11], in material group A, was classified as being in the "damage tolerance" regime according to the same authors. This singular point, however, is well correlated with the data points in Gruffel *et al.* [7] with a similar grain size in the same material group A, following the predicted slope as given by Equation 2. This correlation indicates that the "damage tolerance" regime is identical to the "superplastic-crack growth" regime as classified in this paper.

3.2. Factors influencing tensile ductility of alumina at a given stress

As can be seen in Fig. 2, large differences in tensile ductility are obtained in Regime IV depending on the specific alumina material studied. This figure also includes data for alumina containing 40 wt % Y-TZP taken from Wakai *et al.* [9]. The differences in tensile ductility observed can be explained through an understanding of the factors controlling fracture in polycrystalline ceramics as viewed from the fracture mechanics model, Equation 2. Because the grain size is a variable which strongly influences the tensile ductility, it was decided to plot the data in Regime IV as a function of grain size. The results are shown in Fig. 3 where ε_f is plotted as a function of the logarithm of grain size. Excellent agreement between experimental data and Equation 2 was found for alumina containing a small amount of MgO, where the grain sizes vary from 0.66–1.5 μm as can be seen with the lowest curve in the figure. That is, the predicted slope based in Equation 2 is nearly equal to the experimentally observed slope. Although the data in Fig. 3 indicate a good correlation between the fracture strain and grain size for dilutely alloyed alumina, other factors are seen to contribute to the fracture strain. Thus, the tensile ductility, at a given grain size, is seen to increase with solid solution additions of MgO and with large additions of the second-phase zirconia. This difference in tensile ductility between various alumina material groups can be mainly attributed to the difference in the critical stress intensity factor, K_c, according to Equation 2. Thus, it can be concluded that the value of K_c of alumina increases with increasing amounts of MgO or zirconia. Using the Gilman relation, Equation 1, K_c is seen to be a function of the surface and grain-boundary energies for a given material. From a consideration of these variables, it is predicted that an addition of MgO increases K_c by increasing the surface energy and/or decreasing the grain-boundary energy. This occurs as MgO segregates to the grain boundaries of alumina, altering the grain-boundary structure such that the grain-boundary energy is decreased. In the case of the enhancement of tensile ductility of alumina by zirconia, another explanation is proposed. Increasing the amount of zirconia in alumina results in an increase in the amount of Al_2O_3–ZrO_2 boundaries. It is known that the grain-boundary energy for the Al_2O_3–ZrO_2 interface is lower than that for the Al_2O_3–Al_2O_3 interface [40]. Thus, K_c is expected to increase with an addition of zirconia to alumina.

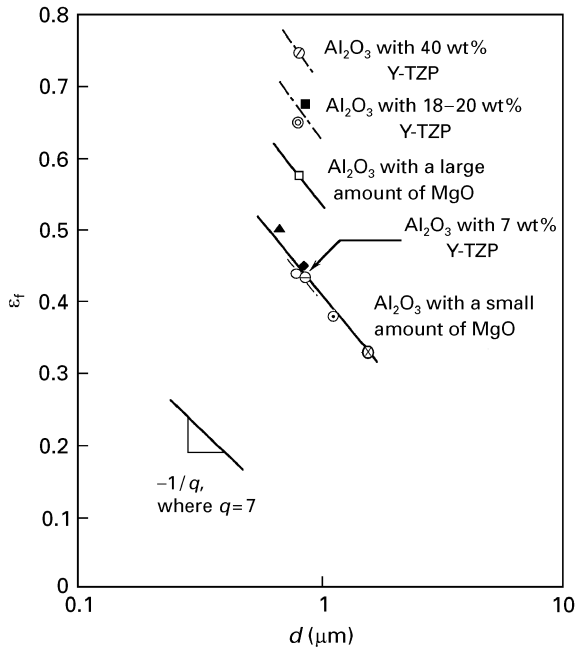

Figure 3 Influence of grain size on the true fracture strain for fine-grained alumina at a given flow stress, 20 MPa. For key; see Table I.

A similar analysis of the tensile ductility reported in the microcracks growth regime (Regime III) was not possible due to lack of sufficient fracture strain data in tension. Limited data do show that the flexure strain values of the alumina material with 0.3 wt % MgO are

* The value of q reported by Kim *et al.* [14], as 4, is not correct. It was measured incorrectly by mistake. The correct value of q is 7.

observed to be higher than the tensile fracture strains of the alumina material with 200 p.p.m. MgO, though the former material has a coarser grain size (Table I). This discrepancy in ductility may be related to the addition of MgO which increases the tensile ductility or to the possibility that the flexure ductility is inherently higher than the tensile ductility at a given flow stress.

4. Conclusions

1. The high-temperature tensile ductility behaviour of polycrystalline fine-grained alumina can be categorized into four regimes, depending on flow stress: (I) fast-crack growth regime, (II) single-crack growth regime, (III) microcracks growth regime, and (IV) superplastic-crack growth regime.

2. A fracture mechanics model applied to interpret the tensile ductility of alumina in Regime IV predicts quantitatively the increase in the true fracture strain with decreasing stress and with decreasing grain size.

3. The enhancement of tensile ductility in alumina by dilute MgO addition is attributed to an increase in the surface energy and/or decrease in the grain-boundary energy.

4. The enhancement of tensile ductility in alumina by the addition of a second phase of zirconia is attributed to an increase in the amount of alumina–zirconia grain boundaries which have a low grain-boundary energy.

Acknowledgement

This work was supported by the Korean Ministry of Education through the New Materials Research Fund in 1996.

References

1. W. D. KINGERY and R. C. COBLE, in "NBS Monograph 59", "Mechanical Behavior of Crystalline Solids", Proceedings of an American Ceramic Society Symposium, (National Bureau of Standards, Washington, DC, 1962) p. 56.
2. E. K. BEAUCHAMP, G. S. BAKER and P. GIBBS, in Report ASD TR, April 1962, Directorate of Materials and Processes (Wright-Palterson Air Force Base, OH, 1962) p. 61.
3. HAROLD J. FROST and MICHAEL F. ASHBY, "Deformation-Mechanism Maps-The Plasticity and Creep of Metals and Ceramics" (Pergamon Press, 1982) p. 98.
4. W. R. CANNON and T. G. LANGDON, *J. Mater. Sci.* **23** (1988) 1.
5. W. R. CANNON and O. D. SHERBY, *J. Am. Ceram. Soc.* **60** (1977) 44.
6. B. J. DALGLEISH, E. B. SLAMOVICH and A. G. EVANS, *ibid.* **68** (1985) 575.
7. P. GRUFFEL, P. CARRY and A. MOCELLIN, in "Science of Ceramics", edited by D. Taylor, Vol. 14 (The Institute of Ceramics, Shelton, Stoke-on-Trent, UK, 1988) p. 587.
8. T. KUROISHI, K. UNO and F. WAKAI, in "Superplasticity", MRS International Meeting on Advanced Materials, Vol. 7, edited by M. Kobayashi and F. Wakai (Materials Research Society, Pittsburgh, PA, 1989) p. 267.
9. F. WAKAI, Y. KODAMA, S. SAKAGUCHI, N. MURAYAMA, H. KATO and T. NAGANO, in "Superplasticity in Advanced Materials", MRS Conference Proceedings, International Meeting on Advanced Materials, edited by M. Doyama, S. S. Somiya, R. P. H. Chang, M. Kobayashi and F. Wakai, Vol. 7 (Materials Research Society, Pittsburgh, PA, 1989) p. 259.
10. D. S. WILKINSON, C. H. CACERES and A. G. ROBERTSON, *J. Am. Ceram. Soc.* **74** (1991) 922.
11. A. G. ROBERTSON, D. S. WILKINSON and C. H. CACERES, *ibid.* **74** (1991) 915.
12. Y. YOSHIZAWA and T. SAKUMA, *Acta Metal. Mater.* **40** (1992) 2943.
13. *Idem.*, *Acta Mater.* in press.
14. W. J. KIM, J. WOLFENSTINE and O. D. SHERBY, *Acta Metall. Mater.* **39** (1991) 199.
15. W. J. KIM, PhD dissertation, Stanford University, Stanford, CA (1993).
16. F. WAKAI, S. SAKAGUCHI and Y. MATSUNO, *Adv. Ceram. Mater.* **1** (1986) 259.
17. Y. MA and T. G. LANGDON, in "Superplasticity in Metals, Ceramics, and Intermetallics", edited by M. J. Mayo, M. Kobayashi and J. Wadsworth, Materials Research Society Symposium Proceedings, Vol. 196 (Materials Research Society, Pittsburgh, PA, 1990) p. 325.
18. T. HERMANSON, K. P. D. LARGERLOF and G. L. DUNLOP, in "Superplasticity and Superplasticity Forming", edited by C. H. Hamilton and N. E. Paton (TMS, Warrendale, PA, 1988) p. 631.
19. T. G. NIEH, C. M. McNALLY and J. WADSWORTH, *J. Metals* **41**(9) (1989) 31.
20. D. J. SCHISSLER, A. H. CHOKSHI, T. G. NIEH and J. WADSWORTH, *Acta Metall. Mater.* **39** (1991) 3227.
21. F. WAKAI and H. KATO, *Adv. Ceram. Mater.* **3** (1988) 71.
22. F. WAKAI, Y. KODAMA, N. MURAYAMA, S. SAKAGUCHI, T. ROUXEL, S. SATO and T. NONAMI, in "Superplasticity in Advanced Materials", edited by S. Hori, M. Tokizane and N. Furushiro (Japan Society for Research on Superplasticity, Osaka, 1991) p. 205.
23. J. G. WANG and R. RAJ, *J. Am. Ceram. Soc.* **67** (1984) 399.
24. F. WAKAI, Y. KODAMA and S. SAKAGUCHI, N. MURAYAMA, K. IZAKI and K. NIHARA, in "Superplasticity in Metals, Ceramics, and Intermetallics", edited by M. J. Mayo, M. Kobayashi and J. Wadsworth, Materials Research Society Symposium Proceedings, Vol. 196 (Materials Research Society, Pittsburgh, PA, 1990) p. 349.
25. F. WAKAI, H. OKAMURA, N. KIMURA and P. DESCAMPS, in "1st Japan international SAMPE Symposium Proceedings", edited by F. Wakai and N. Funeshiro (1989) p. 267.
26. F. WAKAI, Y. KODAMA, S. SAKAGUCHI and T. NONAMI, *J. Am. Ceram. Soc.* **73** (1990) 457.
27. F. WAKAI, Y. KODAMA and T. NAGONO, *Jpn. J. App. Phys. Ser.* 2, *Lattice Defects Ceram.* **28** (1989) 57.
28. XIN WU and I. W. CHEN, *J. Am. Ceram. Soc.* **75** (1992) 2733.
29. T. ROUXEL, F. WAKAI and K. IZAKI, *ibid.* **75** (1992) 2363.
30. W. J. KIM, J. WOLFENSTINE, G. FROMMEYER, O. A. RUANO and O. D. SHERBY, *Scripta Metall.* **23** (1989) 1515.
31. W. J. KIM, J. WOLFENSTINE, G. FROMMEYER and O. D. SHERBY, "Superplastic behavior of Kappa Carbide", *J. Mater. Res.* (1995) submitted.
32. A. S. TETELMAN and A. J. McEVILY, "Fracture of structural Materials" (Wiley, New York, 1967) p. 52.
33. J. J. GILMAN, "Mechanical Behavior of Crystalline Solids", National Bureau of Standards Monograph 59 (NBS, 1963) p. 79.
34. P. NIKOLOPOULOS, *J. Mater. Sci.* **20** (1985) 3993.
35. J. B. WACHTMAN Jr and D. G. LAM Jr, *J. Am. Ceram. Soc.* **42** (1959) 254.
36. R. RAY and S. BAIK, *Metall. Sci.* **14** (1980) 385.
37. D. S. WILKINSON and V. VITEK, *Acta Metall.* **30** (1982) 1723.
38. M. D. THOULESS, C. H. HSUEH, and A. G. EVANS, *ibid.* **31** (1982) 1675.
39. F. C. MONKMAN and N. J. GRANT, *Proc. ASTM* **56** (1956) 834.
40. I. W. CHEN and L. A. XUE, *J. Am. Ceram. Soc.* **73** (1990) 2585.

Received 5 November 1996
and accepted 17 April 1997